All-Solid State Iron Resonance Lidar for Measurement of Temperature and Winds in the Upper Mesosphere and Lower Thermosphere

R. Collins[0000-0001-7055-1228], J. Li[1][0000-0003-1048-4427]], B. Wiliams[2][0000-0002-1797-5985], B. Kaifler[3][0000-0002-5891-242X], D. Thorsen[1][0000-0002-5358-9846]

[1] Geophysical Institute, University of Alaska Fairbanks, Fairbanks, AK 99775, USA, rlcollins@alaska.edu

[2] GATS Inc , Boulder, CO 80301, USA, b.p.williams@gats-inc.com

[3] Institute of Atmospheric Physics, German Aerospace Center, Oberpfaffenhofen-Wessling, BY, Germany, bernd.kaifler@dlr.de

Abstract. The Arctic atmosphere and subauroral region are a natural laboratory for understanding plasma-neutral and dynamical coupling in the atmosphere and geospace. During geomagnetically active periods the auroral electrojet and auroral precipitation are overhead at the High-Frequency Active Auroral Research Program (HAARP) facility in Gakona, Alaska (62°N, 145°W) and facilitate active experiments. Iron resonance lidar systems are uniquely suited for these active investigations as naturally occurring iron layers extend from the upper mesosphere to the middle thermosphere (~70-150 km). A novel lidar system has been demonstrated at the German Aerospace Center using an Nd:YAG laser that operated at a minor line at 1116 nm and was tripled to the iron resonance line at 372 nm. This prototype laser was fully solid-state without liquid dyes or flashlamps and with diode pumping. We are developing a lidar system based on this prototype system that can operate robustly at the remote location of HAARP. We will employ a diode-pumped Nd:YAG laser with second and third harmonic generation. The laser will be injection-seeded by a tunable diode laser allowing the laser to frequency scan the iron line. The laser pulse spectra will be recorded on a shot-by-shot basis using an etalon imaging system with a spectral reference. The lidar system is will operate at 372 nm, with a pulse repetition rate of 100 pps, a pulse energy of 30 mJ, and a 0.9-m diameter telescope. We present the system specifications and the expected performance of the system.

Keywords: Resonance Lidar, Solid-State, Thermosphere.

1 Introduction

1.1 Radar and Lidar studies at HAARP

The HAARP (High-Frequency Active Auroral Research Program) facility in Gakona, Alaska (62°N, 145°W) has allowed controlled scientific investigation of the ionosphere for over 30 years [1]. However, the inability to measure neutral molecule properties has made it difficult to accurately interpret and model experimental data. In this paper we describe a resonance lidar that is intended to conduct coordinated observations with the established Ionospheric Research Instrument (IRI) at HAARP. The IRI can operate as both a Radio Frequency heater as well as a radio transmitter. A wind-temperature lidar at Gakona would support studies of the mesosphere, thermosphere and ionosphere in the following areas: Dusty space plasmas with lidar measurements of polar mesospheric clouds, and heater-radar measurements of polar mesospheric summer echoes; Coupling of mesosphere and lower thermosphere with wind measurements through the D- and E-region; Generation of Extremely Low Frequency and Very Low Frequency Waves with measurements of neutral density and temperature.

1.2 Iron Resonance Lidar

Resonance lidar systems provide high-resolution temperature, wind, and metal density measurements in the upper mesosphere and lower thermosphere (~80-110 km) based on the occurrence of the meteoric metal layers at that altitude [2,3,4]. At altitudes below the metal layers, resonance lidar measures Rayleigh scatter that decreases with altitude and yields temperature measurements from 30 km to 70 km [5,6]. The stronger resonant scatter from metal atoms in the D- and lower E-region allows wind, temperature, and metal density measurements that are beyond the ability of current Rayleigh lidars. This combination of lidar techniques have yielded measurements of the atmospheric profile from the stratosphere to the thermosphere (~15-110 km) [7,8].

Measurements with a high-sensitivity resonance lidar at McMurdo, Antarctica (78°S, 167°E) have revealed the extension of the neutral iron layer upward from the “traditional” altitudes of the MLT (~70 km-110 km) to an “extended” upper altitude of 170 km [5]. This extension has yielded measurements of temperature profiles in the E-region above 150 km. Lidar observations made during auroral activity (Kp ~ 6) documented the increase in neutral temperature associated with Joule heating during this geomagnetic storm. These extended neutral iron layers are observed commonly at McMurdo, with iron detected above 130 km over 25% of the time.

The more common appearance of iron than sodium is consistent with the higher abundance of iron in the thermosphere and faster electron-ion recombination rates for iron than sodium [11]. Observations of iron and sodium in Alaska with less sensitive broadband lidars confirm the Antarctic observations. Observations have shown that sporadic iron layers appear at altitudes above the traditional (or main) iron layer when sodium layers do not and that iron is present in the 140 km to 150 km altitude range (Figure 1). A contemporary iron-resonance wind-temperature lidar is uniquely suited to investigating the polar ionosphere-thermosphere through the height of the E-region in the polar regions.

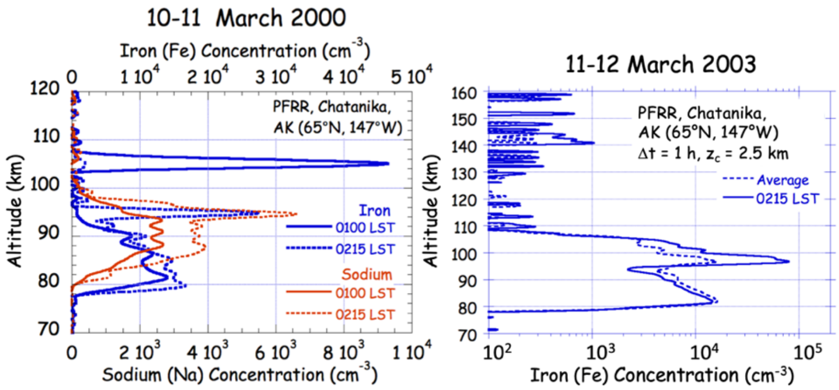

Fig. 1. Left: Lidar measurements showing coincidence of sporadic sodium and iron layers in the D-region (95 km) and presence of iron alone in the E-region (105 km). Right: Lidar measurements showing iron extending into the E-region (140 -150 km) above the traditional iron layer.

2 Iron Resonance Wind-Temperature Lidar

2.1 Spectroscopy of Nd:YAG

The spectroscopic and mechanical properties of Neodymium-doped Yttrium Aluminum Garnate (Nd:YAG: Nd^{3+}:$Y_3Al_5O_{12}$) make it an ideal laser material [12]. The $^4F_{3/2}$ Stark level manifold serves as the upper level for emission lines at 946 nm 1064 nm, 1112 nm, 1116 nm, 1123 nm, and 1319 nm [13] (Figure 2). The 1116 nm transition has upper and lower energy levels in the same manifolds as the familiar 1064 nm transition, but a stimulated emission cross section that is an order of magnitude smaller than that of the 1064 nm line (~3×10^{-23} m^2).

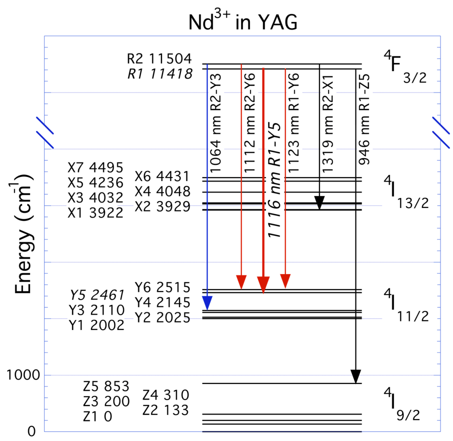

Fig. 2. Partial energy level diagram and transitions of Nd^{3+} in YAG.

2.2 Prototype Nd:YAG-Based Iron Lidar

Serendipitously, the 1116 nm Nd:YAG line lies close to the tripled iron absorption line at 372 nm. A proof-of-principle iron resonance lidar system was demonstrated with a prototype laser optimized for operation at 1116 nm at 100 pps [14]. This prototype laser had a linear stable cavity with a cavity length of 80 cm incorporating an external cavity diode seed laser, diode pumping, and second harmonic and third harmonic generation (Figure 3). The laser was designed to suppress lasing at 1064 nm while allowing lasing at 1116 nm. A thin film polarizer was used to couple the seed laser into the laser cavity. The laser used the twisted-mode technique with a single Nd:YAG rod and a pair of quarter-wavelength plates to support single-mode operation. One of the end mirrors was mounted on a piezoelectric transducer to allow matching of the cavity length to the mode of the seed laser. The output coupling was implemented as a variable beam-splitter using the combination of a half-wavelength plate and the thin film polarizer. The cavity end mirrors were > 99.8% reflective at 1116 nm and < 5% and < 20% reflective at 1064 nm and 1319 respectively. The waveplates were anti-reflection (AR) coated at 1116 nm < 0.1 %. A cavity etalon suppressed the 1112 nm and 1123 nm lines. The second harmonic and third harmonic generation used Type I/II phase matching with a Lithium Triborate (LBO) crystals that were AR coated at 1116 nm (SHG, THG), 558 nm (SHG, THG) and 372 nm (THG). The laser linewidth at 372 nm had a value between 30 MHz and 79 MHz. The laser yielded an output power of 0.5 W at 372 nm. The prototype laser was incorporated into a lidar system and yielded observations of the mesospheric iron layer in November 2015. These first observations also demonstrated the ability to resolve the spectrum of the iron absorption line at sub-Doppler resolution based on the resonance lidar signal.

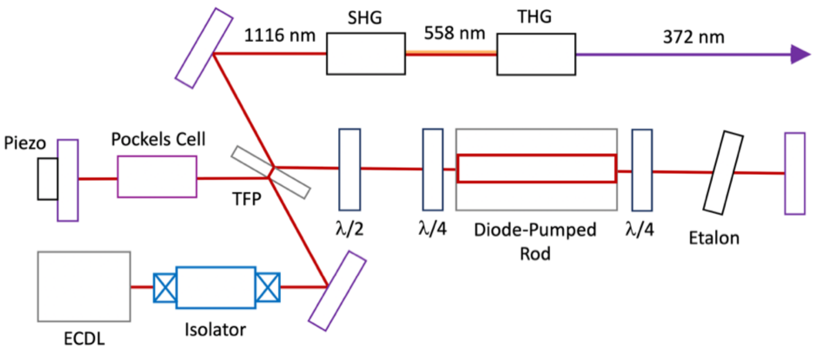

Fig. 3. Schematic of the prototype 1116 nm/372 nm laser system. TFP: Thin film polarizer, ECDL: External cavity diode. SHG: Second harmonic generator. THG: Third harmonic generator.

2.3 New Nd:YAG-Based Iron Lidar

Building on the prototype, we are designing a Nd:YAG laser operating at 1116 nm that employs a dual rod oscillator. A dual-rod architecture provides higher cavity gain and less thermal distortion than a single-rod design. The cavity may also adopt a U-shaped configuration. The U-shaped configuration would include turning mirrors that would be coated to provide further support of lasing at 1116 nm and suppression of 1064 nm. The U-shaped configuration would also support an increase in cavity length with longer laser longer pulse length and decrease in peak pulse power. We will investigate the use of amplifier stages to increase the output optical power. The ramp-and-fire technique will be investigated to maintain single-frequency operation [15].

We estimate the performance capabilities of the lidar based on the expected signals and the associated photon noise [16]. The expected performance is tabulated in Table 1. For the daytime performance of the lidar the receiver includes a double etalon system with an effective bandwidth of 3 pm similar to established iron resonance temperature lidars [17].

Table 1. Nd:YAG Based Iron Resonance Wind-Temperature Lidar.

Transmitter	
Material	Nd:YAG
Wavelength	372 nm
Pulse Energy	30 mJ
Repetition Rate	100 pps
Linewidth	50 MHz
Receiver	
Telescope Diameter	0.91 m
Resolution	
Temporal (night/day)	300 s/600 s
Range (night/day)	1000 m/2000m
Measurement Uncertainty	
Iron Concentration (night/day)	0.6 %/0.5 %
Temperature (night/day)	2 K/5 K
Wind (night/day)	2 m/s/5 m/s

Acknowledgements

The development of the new iron resonance wind-temperature lidar is supported by the US National Science Foundation under grants 2048628 and 2048810.

References

1. Pedersen, T.: HAARP, the most powerful ionosphere heater on Earth. Physics Today 68(12), 72-73 (2015).
2. Chu, X., Papen, G. C.: Resonance fluorescence lidar for measurements of the middle and upper atmosphere. In: Fujii, T. T., Fukuchi, T. (eds.), Laser Remote Sensing. pp 179-432, Taylor and Francis, London (2005).

3. Gardner, C. S., & Collins R. L.: Lidar Resonance. In: North, G. R. J. Pyle, J., F. Zhang, F.(eds), Encyclopedia of the Atmospheric Sciences, pp 305-308, Academic Press, Cambridge, (2015).
4. Krueger, D. A., She, C.-Y., Yuan, T.:. Retrieving mesopause temperature and line-of-sight wind from full-diurnal-cycle Na lidar observations. Applied Optics 54(32), 9469-9489 (2015).
5. Chu, X., Yu, Z., Gardner, C. S., Chen, C., Fong, W: Lidar observations of neutral Fe layers and fast gravity waves in the thermosphere (110–155 km) at McMurdo (77.8°S, 166.7°E) Antarctica. Geophysical Research Letters 38(23), L23807 (2011).
6. Collins, R. L., Lehmacher, G. A., Larsen, M. F., Mizutani, K.: Estimates of vertical eddy diffusivity in the upper mesosphere in the presence of a mesospheric inversion layer. Annales Geophysicae 29, 2019-2029 (2011).
7. Dou, X. K., Qiu, S. C., Xue, X. H., Chen, T. D., Ning, B. Q.: Sporadic and thermospheric enhanced sodium layers observed by a lidar chain over China. Journal of Geophysical Research Space Physics 118(10), 6627–6643 (2013).
8. Kopp, M., Gerding, M., Höffner, J., Lübken, F.-J: Tidal signatures in temperatures derived from daylight lidar soundings above Kühlungsborn (54°N, 12°E). Journal of Atmospheric and Solar-Terrestrial Physics 127(), 35-50 (2015).
9. Chu, X., Yu, Z.: Formation mechanisms of neutral Fe layers in the thermosphere at Antarctica studied with a thermosphere-ionosphere Fe/Fe+ (TIFe) model. Journal of Geophysical Research Space Physics 122(6), 6812- 6848 (2017).
10. Chu, X., Nishimura, Y., Xu, Z., Yu, Z., Plane, J. M. C., Gardner, C. S., Ogawa, Y.: First simultaneous lidar observations of thermosphere- ionosphere Fe and Na (TIFe and TINa) layers at McMurdo (77.84°S, 166.67°E), Antarctica with concurrent measurements of aurora activity, enhanced ionization layers, and converging electric field. Geophysical Research Letters, 47(20), 1-10 (2020).
11. Plane, J. M. C., Feng, W., Dawkins, E. C. M.: The mesosphere and metals: chemistry and changes, Chemical Reviews, 115(10), 4497-4541, (2015).
12. Koechner, W.: Solid State Laser Engineering. 6th edn. pp 747. Springer, New York, (2006).
13. Singh, S., Smith, R. G., van Uitert, L. G.: Stimulated-emission cross section and fluorescent efficiency of Nd^{3+} in yttrium aluminum garnet at room temperature. Physical Review B, 10(6), 2566-2572 (1974).
14. Kaifler, B., Büdenbender, C., Mahnke, P., Damm, M., Sauder, D., Kaifler, N., Rapp, M.: Demonstration of an iron fluorescence lidar operating at 372 nm wavelength using a newly-developed Nd:YAG laser. Optics Letters, 42(15), 2858-2861(2017).
15. Henderson, S. W., E. H. Yuen, Fry, E. S.: Fast resonance-detection technique for single-frequency operation of injection-seeded Nd:YAG lasers, Optics Letters 11(11), 715-717 (1986).
16. Gardner, C. S.: Performance capabilities of middle-atmosphere temperature lidars: comparison of Na, Fe, K, Ca, Ca+, and Rayleigh systems, Applied Optics, 43(25) 4941-4956, (2004).
17. Chu, X., Pan, W., Papen, G. C., Gardner, C. S., Gelbwachs, J. A.: Fe Boltzmann temperature lidar: design, error analysis, and initial results at the North and South Poles, Applied Optics, 41(21), 4400-4410 (2002).